Diagnosis of the Heavy Rain near a Meiyu Front Using the Wet Q Vector Partitioning Method

YUE Caijun* (岳彩军), SHOU Shaowen (寿绍文), LIN Kaiping (林丌平), and YAO Xiuping (姚秀萍)

Department of Atmospheric Sciences, Nanjing Institute of Meteorology, Nanjing 210044

ABSTRACT

A heavy rain process of the Changjiang–Huaihe Meiyu front (MYF) is diagnosed by the agency of the traditional Q vector partitioning (QVP) method to decompose the wet Q vector (Q) in a natural coordinate system that follows the isoentropes and by using the numerical simulation results of the revised MM4 meso-scale model. The technique shows that the partitioned wet Q vectors can lead to a significant scale separation of vertical motion related to the torrential rain. The results not only verify the existing conclusion that different scales interact throughout the rainstorm but also indicate the largely different roles of these scales during differing phases of the heavy rainfall on a quantitative basis. Specifically, during the developing stage, the large-scale plays a predominant role in forcing vertical motion, while frontal-scale forcing is secondary; during the intense stage, the frontal-scale evolves into the primary factor of forcing vertical motion, whereas the large-scale forcing is minor and plays a diminishing role and can even be ignored; and during the decaying stage, the large-scale once again serves as the main forcing of vertical motion in such a way that the forcing of the frontal-scale decays quickly and is of secondary importance. Furthermore, the partitioned wet Q vectors are suggested to be more suitable than the total wet Q vector for evaluating the potential physical mechanism of rainstorm genesis. The first step is that the forcing of large-scale $2\nabla \cdot Q_s^*$ gives rise to the genesis of meso-scale $2\nabla \cdot Q_n^*$ forcing; and then, accordingly as $2\nabla \cdot Q_n^*$ forcing increases, whereby the secondary circulation is reinforced, the intensity of the rainfall is strengthened; and at last, the secondary circulation caused by $2\nabla \cdot Q_n^*$ forcing is directly responsible for generation of the MYF heavy rainfall.

Key words: wet Q vector partitioning, wet Q vector, Meiyu front heavy rainfall, interaction of different scales, diagnosis

1. Introduction

The Q vector has been used widely in operational jobs and studied theoretically since it was depicted by Hoskins et al. (1978). In particular, in entering the 1990s, the fact that the concepts of semi-geostrophic Q vector, C vector, ageostrophic Q vector, and wet Q vector are proposed in turn shows that the theoretical study of the Q vector has been considerably perfect (Yue, 1999). In scientific documents, the Q vector approach is granted as an advanced method to evaluate vertical motion on an operational basis (Dunn, 1991), and appears to provide one of the best means of calculating vertical motions numerically (Durran and Snellman, 1987). Actually, Q vector partitioning (QVP) has more application value to diagnosis. Studies from outside China have delineated that QVP is a useful tool to investigate physical process of frontogenesis and vertical motion, insomuch as partitioning

can separate processes and structure of meteorological interest which are difficult to display only by a "total" Q vector. The traditional decomposition of the Q vector in a natural coordinate system that follows isentrope was reported by Hoskins et al. (1978) and Keyser et al. (1988). Davies–Jones (1991) obtained a Q vector partitioning that has the notable property of being "intrinsic" — that is, independent of any reference system — thereby examining the frontogenetical forcing of secondary circulations. Keyser et al. (1992) not only arrived at a similar conclusion but also found that the decomposition of the Q vector into along- and cross-isentrope components leads to an interesting scale separation of the vertical motion pattern associated with a baroclinic disturbance, suggesting an interpretation of the characteristic comma structure of vertical motion in middle latitude baroclinic disturbances when he diagnosed the output from an idealized

*E-mail: yuecaijun2000@163.com

synoptic model. QVP is widely used in the synoptic literature, e.g., Kurz (1992) analyzed the frontogenesis and cyclogenesis processes. Barnes and Colman (1993) diagnosed a storm occurring in northeast Colorado on Christmas in 1987 and gave a clear account of the appearance of the largest secondary vorticity developing a main vortex in the synoptic process. In addition, Schar and Wernli (1993) utilized a partitioning that is essentially the same as that of Davies–Jones. Martin (1999) also adopted a decomposition of the Q vector along isentropes, which is different from that employed by Keyser et al. (1992), to diagnose the upward motion in an occluded cyclone. Morgan (1999) applied QVP to diagnose surface frontogenesis and vertical motion. Generally, the Q vector is decomposed into a natural coordinate system that follows isentropes , but Jusem and Atlas (1998) proposed a new partitioning that consists of splitting the Q vector into along- and cross-isohypse components. In particular, the Q vector is partitioned in the natural coordinate system that follows the geostrophic wind, and an important conclusion can be drawn by applying the new QVP to a gridding analysis of a real weather situation. The previous analyses show that studies from outside China on QVP are abundant concerning its application to diagnose different synoptic processes and reveal their potential physical mechanisms, which are difficult to exhibit by "total" Q. In brief, the works primarily point to quasi-geostrophic QVP and its application. Till now, the partitioning of the wet Q vector and its applications at home and abroad have not been explored in such a manner, which is the point of this paper.

In previous studies, QVP is only adopted to deal with a quasi-geostrophic Q vector so that it only displays the forcing mechanism of vertical motion related to large-scale and quasi-geostrophic synoptic processes as usual. However, its limited application is due to its partitioning. The latest results portray that the quasi-geostrophic Q vector has far less diagnostic abilities in comparison to the wet Q vector in the context of the study of rainstorm generation from the meso-scale Meiyu front (MYF) in the Changjiang–Huaihe basins (Yue and Shou, 2002). Additionally, Tao (1980) suggested that a rainstorm is a result of the interactions of different scale synoptic systems, even though it is a

meso-scale phenomenon, and a meso-scale system directly produces heavy rainfall genesis and plays a key role in the interactions of differing scales. The study by Yang et al. (1987a, b) was devoted to the meso-α scale rainband from MYF with its characteristics and genesis mechanism and gave a dynamical analysis. Si et al. (1995) addressed the relation of the change of large-scale circulation to the change of the frontal features and frontal rainfall environment. Although multi-scale interactions in hard rainfall process have been examined greatly and depicted and discussed in detail (Tao, 1980; Xue and Liu, 1996), no one has done so with the aid of wet Q vector partitioning (WQVP) on a quantitative basis in China or abroad till now. What roles do the large- and meso-scales play in the MYF torrential rain process respectively? This question will be investigated in the following discussion. The approach of splitting the quasi-geostrophic Q vector is used to decompose the wet Q vector, which, in turn, is utilized to diagnose vertical motion in relation to the MYF rainstorm process, thereby disclosing how vertical motion is excited and forced by different scales throughout the heavy rainfall process.

2. Data and methods

2.1 Data

Owing to rare observations (there are only 2000 Beijing Time (BT) 5 July, 0800 BT and 2000 BT 6 July 1991) , making diagnosis inconvenient, and the revised MM4 model employing strong simulation (Dong et al., 2001a, b), we take 2000 BT 5 July and 0800 BT 6 July 1991 as original fields and integrate 12 hours respectively with synchronous real data to examine each corresponding counterpart of the simulation. In consequence, we find that the observations and simulations are roughly in agreement on a high field basis, which shows that the simulations are so reliable that they can be used as diagnostic data. In order to improve the true effect of the analysis, we still make use of the observations and interpose three times simulations between each two observations, so there are nine times used data. Evidently, the diagnostic data are remarkably intensive, whereby it is favorable to study it in full with related precipitation.

2.2 Methods

2.2.1 Wet Q vector and ageostrophic omega equation (Zhang, 1998)

The expression of the wet Q vector in the P-coordinate system is

$$Q^* = (Q_x^*, Q_y^*) = \left\{ \frac{1}{2}\left[f\left(\frac{\partial v}{\partial p}\frac{\partial u}{\partial x} - \frac{\partial u}{\partial p}\frac{\partial v}{\partial x}\right) - h\frac{\partial V}{\partial x}\cdot\nabla\theta - \frac{\partial}{\partial x}\left(\frac{LR\omega}{c_p\cdot p}\frac{\partial q_s}{\partial p}\right)\right], \right.$$
$$\left. \frac{1}{2}\left[f\left(\frac{\partial v}{\partial p}\frac{\partial u}{\partial y} - \frac{\partial u}{\partial p}\frac{\partial v}{\partial y}\right) - h\frac{\partial V}{\partial y}\cdot\nabla\theta - \frac{\partial}{\partial y}\left(\frac{LR\omega}{c_p\cdot p}\frac{\partial q_s}{\partial p}\right)\right]\right\}, \qquad (1)$$

where, $h = (R/p)(p/1000)^{R/c_p}$, subscripts x and y denote zonal and latitudinal components respectively, and the other symbols are usual in meteorological physics. Recently, Yao and Yu (2000; 2001) derived a formula similar to Eq. (1) by another way.

The ageostrophic omega equation whose forcing term is the wet Q vector divergence in the P-coordinate system is

$$\nabla^2(\sigma\omega) + f^2 \frac{\partial^2 \omega}{\partial p^2} = -2\nabla \cdot Q^* . \quad (2)$$

When the omega field employs a wave feature, Eq. (2) gives:

$$\nabla \cdot Q^* \propto \omega, \quad (3)$$

and Eq.(3) can be used to diagnose vertical motion. Thus, if $\nabla \cdot Q^* < 0$ ($\nabla \cdot Q^* > 0$), then $\omega < 0$ ($\omega > 0$), namely, upward (downward) motion.

2.2.2 The partitioning of the wet Q vector

The specific partitioning is illustrated with the aid of Fig. 1.

Based on the traditional QVP, we decompose the wet Q vector in a natural coordinate system that follows the isentropes (Fig. 1), where $\vec{n}$ is the unit vector in the direction of $\nabla\theta$, which is given by $\vec{n} = \frac{\nabla\theta}{|\nabla\theta|}$, s is 90° counterclockwise from n, i.e., $s = k \times n$. For convenience, the "total" wet Q vector is referred to as Q_{total}^* (which is equal to Q^*), so the component of Q^* in the direction of $\vec{n}$ will be denoted as Q_n^* and is equal to

$$Q_n^* = \left(\frac{Q^* \cdot \nabla\theta}{|\nabla\theta|} \right) \frac{\nabla\theta}{|\nabla\theta|}$$

or

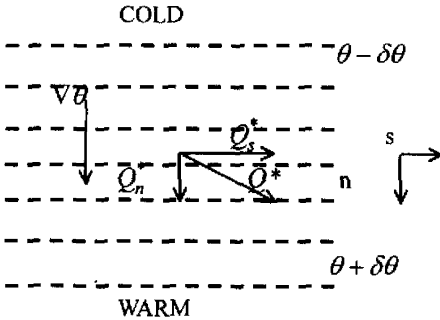$$Q_n^* = \left(\frac{Q^* \cdot \nabla\theta}{|\nabla\theta|} \right) n .$$

Fig. 1. Schematic describing the natural coordinate partitioning of the wet Q vector used in this study. Dashed lines are isentropes on an isobaric surface. Here $Q_n^*(Q_s^*)$ is the component of $Q^*(Q_{\text{total}}^*)$ in the $\vec{n}(\vec{s})$ direction.

The component of Q^* in the direction of $\vec{s}$ will be denoted as Q_s^* and is equal to

$$Q_s^* = \frac{Q^* \cdot (k \times \nabla\theta)}{|\nabla\theta|} \left[\frac{(k \times \nabla\theta)}{|\nabla\theta|} \right] .$$

Obviously, $Q^* = Q_n^* + Q_s^*$. The component Q_n^* is in the cross-isentrope direction with a quasi-geostrophic deviation feature, related to frontogenesis and frontology and reflecting the meso-scale information. The component Q_s^* is in the along-isentrope direction (namely, the thermal wind direction) with a quasi-geostrophic feature and reflecting the large-scale information. Both Q_n^* and Q_s^* have the same diagnostic characteristics as Q^*, and what is more, Q_n^* and Q_s^* are associated with meso- and large-scale forcing respectively (Keyser et al., 1988; Davies-Jones, 1991; Keyser et al., 1992; Kurz, 1992; Barnes and Colman, 1993; Schar and Wernli, 1993; Martin, 1999; Morgan, 1999). As the ω field has a wave feature, there is $\nabla \cdot Q_n^*(\nabla \cdot Q_s^*) \propto \omega$, which can be utilized to diagnose vertical motion. If $\nabla \cdot Q_n^* < 0$ ($\nabla \cdot Q_s^* < 0$), then $\omega < 0$, which is ascent motion forced by meso- (large-) scale convergence, and vice versa.

3. Precipitation overview

There is a typical Changjiang–Huaihe MYF heavy rainfall event beginning at 2000 BT 5 July 1991, lasting for 24 h. The MYF cyclone developing stage is at about 2000 BT 5 July 1991 when the precipitation just occurs. Subsequent to 2000 BT 5 July and prior to 0800 BT 6 July 1991 the rainfall becomes strong by degrees. An apparent turnabout shows up at 0800 BT 6 July when a noticeable cyclone appears in the Changjiang–Huaihe basins with the rainfall growing greatly. After 0800 BT and before 2000 BT 6 July the precipitation is the strongest with intensive distribution on a spatial and temporal basis associated with the strongest cyclone having typical meso-scale characteristics. At about 2000 BT 6 July 1991, the cyclone moves eastward to the sea, relating to the end of the precipitation. Seeing that the real rain area extends from 29.25°N to 38.80°N and 109.717°E to 126.33°E, the range is the predominant diagnostic region while other belts are not considered in this paper.

4. Specific application of WQVP

Studies have shown that the 700 hPa convergence field of the wet Q vector divergence is in good relation to the fallout band and intensity of the rainstorms from MYF (Yue and Shou, 2002). As a consequence, the problem can be solved by the analysis of the 700 hPa wet Q vector divergence pattern. The specific diagnosis will be given in the following text.

4.1 From 2000 BT 5 July to 0800 BT 6 July

Based on the distribution of the 700 hPa Q vector divergence fields at 2000 BT, 2300 BT 5 July and 0200 BT, 0500 BT 6 July (figures omitted), we can see that

the distribution characteristics of the convergence region with its center of Q_s^* vector divergence correspond well to the counterparts of Q_{total}^* in comparison to Q_n^*. Moreover, some convergence cores of Q_{total}^* vector divergence can rarely be reflected by the counterparts of Q_n^* in the corresponding location. This suggests that $2\nabla \cdot Q_s^*$ ($2\nabla \cdot Q_n^*$) makes up the chief (secondary) component of $2\nabla \cdot Q_{total}^*$, namely the large- (frontal-) scale plays a primary (minor) role in forcing vertical motion during this stage, particularly at 2300 BT 5 July (Fig. 2).

In Fig. 2a, two Q_{total}^* vector divergence convergence centers which are located at (111.3°E, 32.8°N) and (112°E, 33°N) with intensities of -3.62×10^{-15} hPa^{-1} s^{-3} and -4.75×10^{-15} hPa^{-1} s^{-3}, respectively, are reflected well by the corresponding counterparts of the Q_s^* in Fig. 2c with intensities of -2.71×10^{-15} hPa^{-1} s^{-3} and -3.31×10^{-15} hPa^{-1} s^{-3} in such a manner that are reflected poorly by the associated counterparts of the Q_n^* in Fig. 2b with an intensity of -2.31×10^{-15} hPa^{-1} s^{-3}. Notably, the Q_{total}^* vector divergence convergence core, which is located at (113.1°E, 30.8°N) with an intensity of -4.38×10^{-15} hPa^{-1} s^{-3} in Fig. 2a is reflected very clearly by the counterpart of Q_s^* in Fig. 2c with an intensity of -3.14×10^{-15} hPa^{-1} s^{-3} while it is reflected by the weak counterpart of Q_n^* in Fig. 2b only with -1.75×10^{-15} hPa^{-1} s^{-3}. In addition, the convergence intensity of Q_s^* (-5.26×10^{-15} hPa^{-1} s^{-3}) is stronger than its counterpart of Q_n^* (-4.84×10^{-15} hPa^{-1} s^{-3}) within the context of the reflecting counterpart of Q_{total}^* whose center is located at (111.1°E, 29.8°N). All of these indicate that Fig. 2c is better than Fig. 2b to reflect Fig. 2a, and $2\nabla \cdot Q_s^*$ is the main component of $2\nabla \cdot Q_{total}^*$ in such a fashion that $2\nabla \cdot Q_n^*$ constitutes little proportion.

The synchronous high pattern (figures omitted) shows that the Changjiang–Huaihe MYF cyclone develops gradually from 2000 BT 5 July to 0800 BT 6 July 1991, ad interim, hourly precipitation (figures not shown) becomes strong little by little only with a small range of increase during this stage. By means of WQVP and comparison of 700 hPa wet Q vector divergence distribution, we can see that on this stage, the large- (meso-) scale plays the chief (secondary) role in forcing vertical motion, which, with the aid of the wet Q vector partition, reveals that different scales play different roles in the developing stage of MYF cyclones whereas it is difficult for the "total" wet Q vector to show this.

4.2 0800 BT 6 July

By comparing the 700 hPa Q_{total}^* vector divergence convergence field with the counterparts of Q_n^* and Q_s^* at 0800BT 6 July 1991 respectively (figures omitted), we find that in the vicinity of 32.5°N there is a west-east convergence belt of Q_{total}^* vector divergence with three cores at (32.5°N, 114.5°E), (32.5°N, 116.5°E),

and (32.5°N, 119°E), which are reflected well by the counterpart of Q_n^* but only partly by the counterpart of Q_s^*. Additionally, the distribution features of the convergence of the Q_n vector divergence near 30°N is similar to the related counterpart of Q_{total}^*. All of this shows that the meso- (large-) scale explains the main (minor) component of $2\nabla \cdot Q_{total}^*$ and plays a primary (secondary) forcing role in this stage.

In the meanwhile, a mature cyclone turns up in the Changjiang–Huaihe basins and precipitation increases greatly with its intensity stronger than before (figures omitted). In such a case, by virtue of WQVP and the 700 hPa wet Q vector divergence field comparison, we conclude that the forcing of the large- and frontal-scales being responsible for vertical motion has radically changed in this stage in comparison to the previous stage, namely, the frontal-scale forcing in the context of vertical motion associated with MYF heavy rain is predominant and the counterpart of the large-scale is secondary. The great change can be revealed clearly by WQVP whereas it is difficult to find the mechanism of its inner variation in terms of the "total" wet Q vector.

4.3 Between 0800 BT and 2000 BT 6 July

The features of divergence and convergence of the Q vector divergence on the east of 114°E are very similar on the basis of comparing Fig. 3a to Fig. 3b. Specifically, the Q_{total}^* vector divergence convergence band, which is composed of the two convergence cores located at (116°E, 33°N) and (117.5°E, 32.5°N) with intensities of -3.02×10^{-15} hPa^{-1} s^{-3} and -2.98×10^{-15} hPa^{-1} s^{-3} respectively (Fig. 3a), can be reflected well by the counterpart of Q_n^* whose center is located at (116.5°E, 32.8°N) with an intensity of -4.66×10^{-15} hPa^{-1} s^{-3} (Fig. 3b). Apparently, the intensity of the latter is stronger as compared to that of the former, and to some extent the features of the distribution of the Q_s^* vector divergence (Fig. 3c) are poorly related to the counterpart of Q_{total}^* (Fig. 3a), and even contrary. Besides, the Q_{total}^* vector divergence convergence band, which is made up of the centers located at (114.2°E, 31.7°N) and (116.1°E, 31.5°N) with intensities of -3.53×10^{-15} hPa^{-1} s^{-3} and -4.18×10^{-15} hPa^{-1} s^{-3} respectively, can be reflected by the counterpart of Q_n^* which consists of cores located at (113.8°E, 32.5°N) and (115.9°E, 32.5°N) with intensities of -4.5×10^{-15} hPa^{-1} s^{-3} and -4.17×10^{-15} hPa^{-1} s^{-3}, while it can hardly be reflected by the counterpart of Q_s^*. All of this shows that $2\nabla \cdot Q_{total}^*$ includes a larger component of $2\nabla \cdot Q_n^*$ than of $2\nabla \cdot Q_s^*$, namely the forcing of the frontal-scale is much larger as opposed to the large-scale, and the latter plays a background role in such a fashion that the former plays the major role in forcing vertical motion. In addition, analyses of the 700 hPa wet Q vector divergence distribution at 1400 BT and 1700
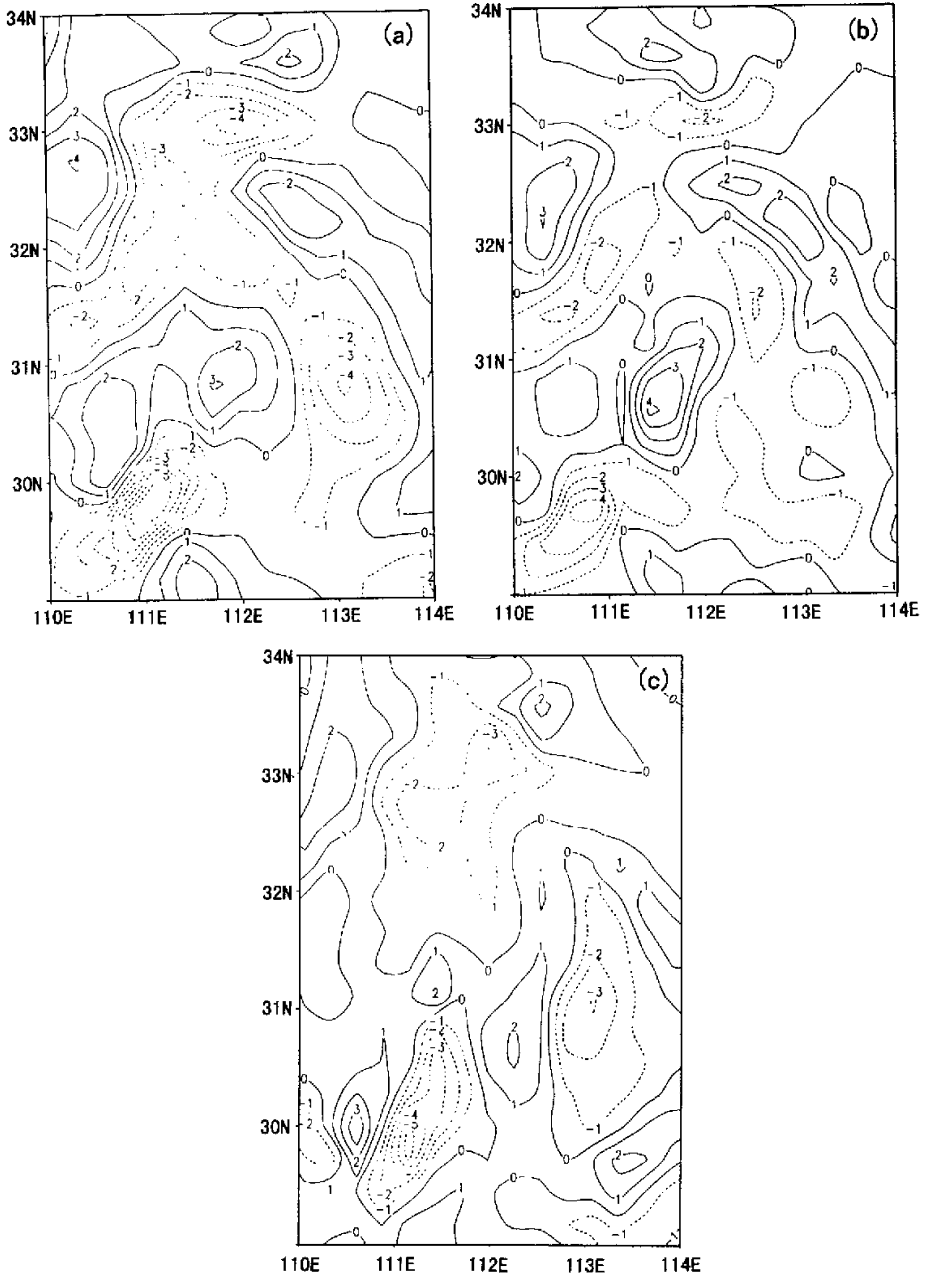
Fig. 2. The distribution of the 700 hPa wet Q vector divergence field at 2300 BT 5 July 1991. Solid (dashed) lines represent divergence (convergence), with units of 10^{-15} hPa^{-1} s^{-3}. Panels (a), (b), and (c) denote $2\nabla \cdot Q^*_{total}$, $2\nabla \cdot Q^*_n$, and $2\nabla \cdot Q^*_s$ respectively, which are calculated by simulations.
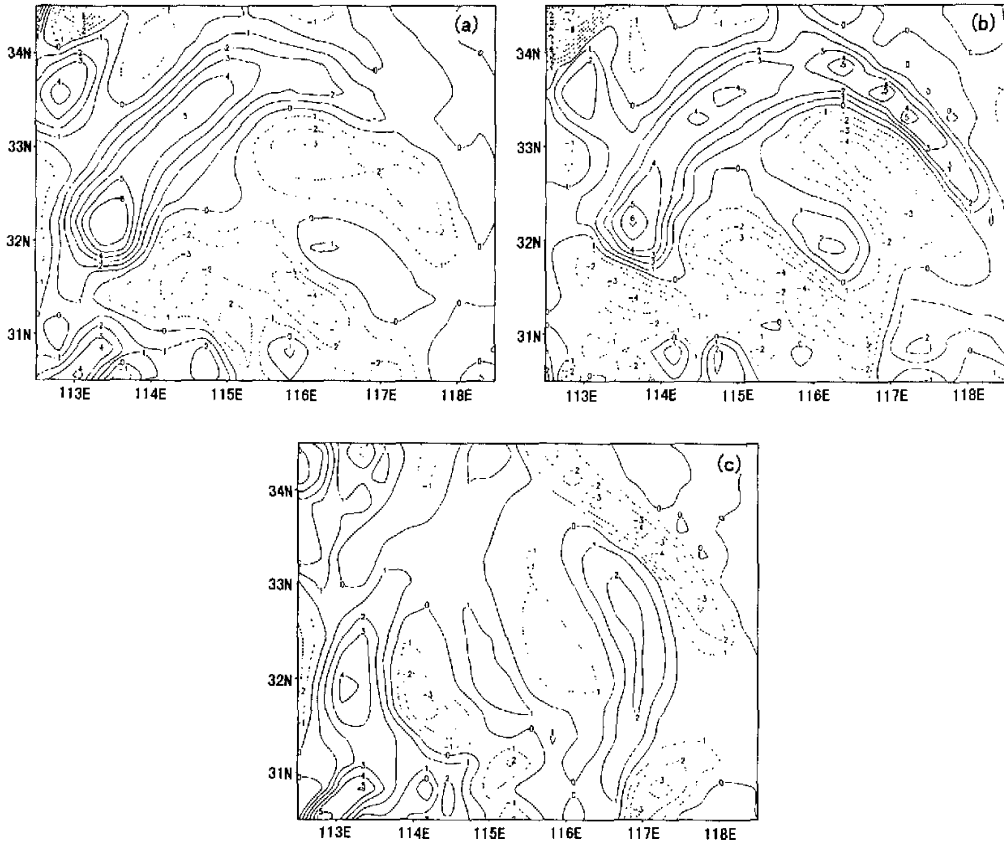
Fig. 3. As in Fig. 2 but for 1100 BT 6 July 1991.

BT 6 July 1991 (figures omitted) can both draw a similar conclusion.

A synchronous high field (figures not shown) reveals that the period from 0800 BT to 2000 BT 6 July 1991 is a strong stage of a MYF cyclone, ad interim, precipitation intensity (figures omitted) greatly increases in the fallout region of concern. By the use of the WQVP analysis, we find clearly that $2\nabla \cdot \boldsymbol{Q}_n^*$ explains the principal component of the "total" wet $\boldsymbol{Q}$ vector divergence field due to the fact that $2\nabla \cdot \boldsymbol{Q}_n^*$ and $2\nabla \cdot \boldsymbol{Q}_{\text{total}}^*$ have a good correspondence within the context of convergence center location and convergence pattern distribution whereas there is great difference between $2\nabla \cdot \boldsymbol{Q}_s^*$ and $2\nabla \cdot \boldsymbol{Q}_{\text{total}}^*$. Furthermore, we also know that in the middle of the MYF strong stage $2\nabla \cdot \boldsymbol{Q}_n^*$ can almost take the place of $2\nabla \cdot \boldsymbol{Q}_{\text{total}}^*$ in such a way that $2\nabla \cdot \boldsymbol{Q}_s^*$ can almost be ignored. From the foregoing, we see that during the strong stage of MYF, the frontal-scale is leading, whereby vertical motion is forced dominantly, and the large-scale is secondary and only plays a background role.

4.4 *2000 BT 6 July*

The convergence intensity of $\boldsymbol{Q}_n^*$ vector divergence is stronger compared to that of $\boldsymbol{Q}_s^*$ over the rain area at 2000 BT 6 July 1991 (figures omitted), which indicates that $2\nabla \cdot \boldsymbol{Q}_s^*$ increases while $2\nabla \cdot \boldsymbol{Q}_n^*$ decreases gradually on the basis of the proportion in $2\nabla \cdot \boldsymbol{Q}_{\text{total}}^*$, in contrast to the previous stage. In other words, large-scale forcing becomes strong and frontal-scale forcing becomes weak by degrees on the basis of vertical motion.

The analysis of the synchronous synoptic chart (figure not shown) shows that a turning point in the life of the cyclone occurs at 2000 BT 6 July 1991 when it has moved eastward to the sea and weakened. Based

on the inter-comparison of the partitioned wet Q vector divergences, we find that in the context of vertical motion, both large- and frontal-scale forcing have smart changes, which are basically the same as their respective counterparts during the developing stage of the MYF cyclone, which, in turn, portrays that the large- (frontal-) scale is getting strong (weak) with the decline of the cyclone.

5. Analysis and discussion

Through the use of WQVP and analysis of a typical Changjiang-Huaihe MYF rainstorm process beginning at 2000 BT 5 July 1991, lasting for 24 h, we not only verify the known result that MYF heavy rainfall is attributed to the multi-scale interactions but obtain new interesting findings as well. Through the developing, maturing, and declining stages of the MYF cyclone, based on the quantification of WQVP, we not only show that the frontal- and synoptic-scales play different roles in differing phases of the heavy rainfall, but we also find clearly that the forcing of the frontal-scale within the context of vertical motion goes from weak to strong and then to weak, and vice versa for the large-scale forcing. Furthermore, WQVP helps us understand further the genesis mechanism of the MYF rainstorm. To be specific, at the beginning stage of the MYF heavy rainfall, the forcing of $2\nabla \cdot Q_s^*$ employing a large-scale feature on the basis of vertical motion is very important, which can excite large range weak ascent motion which causes lower water vapor to rise, and as a consequence, produces the release of vapor condensation latent heat, which, in turn, can make the vertical motion stronger. This occurs under an interactive feedback situation, which leads to sub-synoptic scale secondary circulation genesis. In the strong stage of MYF heavy rainfall, the meso-scale becomes the primary factor forcing the vertical motion, and the meridional secondary circulation excited by $2\nabla \cdot Q_n^*$ with frontal-scale characteristic reaches a vigorous stage, which makes the intensity of rainfall reach its maximum, but the large-scale plays a background role at most. Therefore, we suggest that primarily it is the forcing of large-scale $2\nabla \cdot Q_s^*$ that allows the generation of meso-scale $2\nabla \cdot Q_n^*$ forcing. Then, as the $2\nabla \cdot Q_n^*$ forcing gets strong, whereby the generated secondary circulation reinforces, the intensity of the rainfall increases and, at last, the secondary circulation caused by $2\nabla \cdot Q_n^*$ forcing engenders the genesis of MYF hard rainfall.

6. Summary and concluding remarks

The present study investigates the roles played by large- and meso-scale forcings in a MYF torrential rain process by using the wet Q vector partitioning (WQVP) method. The main conclusions are:

(1) WQVP does a very meaningful job which can disclose the potential mechanisms and physical processes of MYF heavy rainfall genesis which is difficult for the "total" wet Q vector to display.

(2) Splitting the wet Q vector into along- and cross-isentrope components is the cause of a interesting scale separation of vertical motion associated with MYF hard rainfall.

(3) Through the agency of WQVP and comparison of the 700 hPa wet Q vector divergence distribution, we can see clearly that the rainstorm from MYF is generated by the interactions of different scales, and these different scales play different roles in the different stages of the MYF rainstorm. More specifically, during the developing stage, the large-scale plays the predominant role in forcing vertical motion genesis in such a way that the forcing of the frontal-scale is secondary; during the strong stage, the frontal-scale evolves into the primary factor of forcing vertical motion whereas the forcing of the large scale is minor and plays a decreasing role, which can even be ignored during the center of the stage; and during the decline stage, the large-scale once again serves as the main strength of forcing vertical motion while the forcing of the frontal-scale decays quickly and is of secondary importance.

REFERENCES

Barnes, S. L., and B. R. Colman, 1993: Quasigeostrophic diagnosis of cyclogenesis associated with a cut off extratropical cyclone The Christmas 1987 storm. *Mon. Wea. Rev.*, **121**(6), 1613 1634.

Davies-Jones, R., 1991: The frontogenetical forcing of secondary circulations. Part I: The duality and generalization of the Q vector. *J. Atmos. Sci.*, **48**(4), 497 509.

Dong M. Y., Yu W. P., and Shou S. W., 2001a: The improvement and examination of MM4 model cumulus parameterization scheme. Part I: The improvement of MM4 model cumulus parameterization scheme. *Journal of Nanjing Institute of Meteorology*, **24**(1), 66-73. (in Chinese)

Dong M. Y., Yu W. P., and Shou S. W., 2001b: The improvement and examination of MM4 model cumulus parameterization scheme. Part II: The examination of revised model. *Journal of Nanjing Institute of Meteorology*, **24**(2), 228-235. (in Chinese)

Dunn, L. B., 1991: Evaluation of vertical motion: Past, present, and future. *Weather Forecasting*, **6**(1), 65-75.

Durran, D. R., and L. W. Snellman, 1987: The diagnosis of synoptic scale vertical motion in an operational environment. *Weather Forecasting*, **2**(1), 17–31.

Hoskins, B. J., I. Dagbici, and H. C. Daries, 1978: A new look at the ω-equation. *Quart. J. Roy. Meteor. Soc.*, **104**(1), 31–38.

Jusem, J. C., and R. Atlas, 1998: Diagnostic evaluation of vertical motion forcing mechanisms by using Q vector partitioning. *Mon. Wea. Rev.*, **126**(8), 2166–2184.

Keyser, D., M. J. Reeder, and R. J. Reed, 1988: A generalization of Petterssen's frontogenesis function and its relation to the forcing of vertical motion, *Mon. Wea. Rev.*, **116**(3–4), 762–780.

Keyser, D., B. D. Schmidt, and D. G. Duffy, 1992: Quasi-geostrophic vertical motions diagnosed from along- and cross-isentrope components of the Q vector. *Mon. Wea. Rev.*, **20**(5), 731–741.

Kurz, M., 1992: Synoptic diagnosis of frontogenetic and cyclogenetic processes. *Meteor. Atmos. Phys.*, **48**(1), 77–91.

Martin, J. E., 1999: Quasi-geostrophic forcing of ascent in the occluded sector of cyclones and the trowal airstream. *Mon. Wea. Rev.*, **127**(1), 70–88.

Morgan, M. C., 1999: Using piecewise potential vorticity inversion to diagnose frontogenesis. Part I: A partitioning of the Q vector applied to diagnosing surface frontogenesis and vertical motion. *Mon. Wea. Rev.*, **127**(12), 2796–2821.

Schar, C., and H. Wernli, 1993: Structure and evolution of an isolated semi-geostrophic cyclone. *Quart. J. Roy. Meteor. Soc.*, **119**(509), 57–90.

Si, G.-W., K. Kuranoshin, and T. Takeda, 1995: The early summer seasonal change of large-scale circulation over East Asia and its relation to change of the frontal features and frontal rainfall environment during 1991 summer. *Advances in Atmospheric Sciences*, **12**(2), 151–176.

Tao S. Y., 1980: *Chinese Rainstorm*. Science Press, Beijing, 25–32. (in Chinese)

Xue Q. F., and Liu J. L., 1996: The interaction between synoptic scale and sub-synoptic scale in a rainfall process. The Study on Meso-scale Weather and Dynamics, Ding Y. H., Ed., China Meteorological Press, 35–41. (in Chinese)

Yang G. X., Lu H. C., and He Q. Q., 1987a: A meso-α scale study of Meiyu front heavy rain – Part I: Observational studies, *Advances in Atmospheric Sciences*, **4**(3), 264–277.

Yang G. X., Lu H. C., and He Q. Q., 1987b: A meso scale study of Meiyu front heavy rain Part II: The dynamical analysis of rain-band disturbance. *Advances in Atmospheric Sciences*, **4**(4), 485–495.

Yao X. P., and Yu Y. B., 2000: Non-geostrophic wet Q-vector analysis and its application to typhoon torrential rain. *Acta Meteorologica Sinica*, **58**(4), 436–446. (in Chinese)

Yao X. P., and Yu Y. B., 2001: Perfect Q-vector and its diagnoses. *Plateau Meteorology*, **20**(2), 208–213 (in Chinese).

Yue C. J., 1999: The advances on Q vector and its application to synoptic diagnosis. *Meteor. Mon.*, **25**(11), 3–8. (in Chinese)

Yue C. J., and Shou S. W., 2002: Several Q-vectors' comparison. *Journal of Nanjing Institute of Meteorology*, **25**(4), 525–532. (in Chinese)

Zhang X. W., 1998: An expression of the wet Q vector and application. *Meteor. Mon.*, **24**(8), 3–7. (in Chinese)

应用湿Q矢量分解诊断梅雨锋暴雨

岳彩军　寿绍文　林开平　姚秀萍

摘　要

采用传统的Q矢量分解方法将湿Q矢量(Q^*)分解在沿等位温线的自然坐标系中，并结合改进的MM4模式(MMM4)模拟资料，对一次江淮梅雨锋暴雨过程进行诊断分析。结果表明，分解湿Q矢量可将梅雨锋暴雨的垂直运动场进行一个有意义的尺度分离，这不仅验证了梅雨锋暴雨过程中存在不同尺度相互作用的已知结论，而且从定量的角度揭示出不同尺度在梅雨锋暴雨不同阶段所起的作用不同，有明显的主、次之分：在梅雨锋暴雨的开始形成阶段，大尺度对垂直运动场的产生起着主要的强迫作用，锋区尺度的强迫作用处于次要地位；在梅雨锋暴雨的强盛阶段，锋区尺度已经演变为垂直运动场的主要强迫因子，而大尺度的强迫作用则处于次要地位，甚至多起着背景场的作用，其至个别时次可以忽略不计；在梅雨锋暴雨的衰亡阶段，大尺度又逐渐演变为此时垂直运动场的主要强迫动力，而锋区尺度的强迫作用则迅速衰减，其又仅处于次要地位。此外，我们认为分解湿Q矢量比"总"的湿Q矢量更有利于对产生梅雨锋暴雨的潜在物理机制的评估：先是在大尺度$2\nabla \cdot Q_s^*$的强迫作用下诱发中尺度$2\nabla \cdot Q_n^*$强迫作用的产生，随着$2\nabla \cdot Q_n^*$强迫作用的增强，其所强迫作用产生的次级环流增强，降水的强度也同时随着增大，最终由$2\nabla \cdot Q_n^*$强迫作用所产生的次级环流直接导致梅雨锋暴雨的发生。

关键词：湿Q矢量分解，湿Q矢量，梅雨锋暴雨，不同尺度相互作用，诊断